On the Flexural Analysis of Sandwich and Composite Arches through an Isoparametric Higher-Order Model

Sudhakar R. Marur[1] and Tarun Kant[2]

Abstract: A higher-order arch model with seven degrees of freedom per node is proposed to study the deep, shallow, thick, and thin composite and sandwich arches under static loads. The strain field is modeled through cubic axial, cubic transverse shear, and linear transverse normal strain components. As the cross-sectional warping is accurately modeled by this theory, it does not require any shear correction factor. The stress-strain relationship is derived from an orthotropic lamina in a three-dimensional state of stress. The proposed formulation is validated through models with various curvatures, aspect ratios, boundary conditions, materials, and loading conditions.

CE Database subject headings: Sandwich structures; Composite structures; Arches; Static loads.

Introduction

Arches and curved beams made of laminated composite and sandwich materials are being employed extensively in various industries such as automotive, aerospace, energy, medicine, sports, etc., due to their high stiffness to weight ratio, impact strength, etc. Systematic study of composite arches under various static loading conditions is a key to the development of design framework for such structures.

Some of the earlier curved element formulations were based on classical theories, which neglected the transverse shear deformation. Lee (1969) formulated a three-dimensional arch element with six degrees of freedom per node using Castigliano's theorem. Dawe (1974a,b) developed various arch element models by using different orders of polynomial such as cubic, quintic, etc., for tangential and radial displacements and compared the relative merits of these elements. Prathap studied the arch element with linearly interpolated tangential displacement and cubically interpolated radial displacement for field consistency to address membrane locking (Prathap 1985) and variational correctness (Prathap and Shashirekha 1993).

Many elements based on the shear deformable theory of Timoshenko (1921) have been reported in the open literature. Saleeb and Chang (1987) developed a linear and quadratic isoparametric elements based on hybrid-mixed formulation to study arch problems. Mode decomposition technique had been used for developing a locking free isoparametric curved beam element by Stolarski and Chiang (1989). Choi and Lim (1995) developed two- and three-noded curved beam elements based on assumed strain fields and Timoshenko beam theory. Krishnan and Suresh

[1]CSS Foundation, 313 A4 Wing, Cauvery Block, NGH Complex, Koramangala, Bangalore—560047, India. E-mail: srmarur@iitbombay.org
[2]Department of Civil Engineering, Indian Institute of Technology, Powai, Mumbai—400076, India. E-mail: tkant@civil.iitb.ac.in

(1998) formulated a shear deformable curved beam element, with four degrees of freedom per node.

Stolarski and Belytschko (1982) studied the role of reduced integration in removing membrane locking in curved beam elements. Also, they investigated (1983) the shear and membrane locking phenomena in isoparametric finite elements, which are based on displacement, hybrid-stress, and mixed formulations. Babu and Prathap (1986) and Prathap and Babu (1986, 1987) offered key insights as well as the solution to the locking problem for curved beams by introducing field-consistent shear and membrane strain interpolations; also they provided *a priori* error models for locking errors and stress oscillations and confirmed the same through numerical experimentation. Lee and Sin (1994) reported a locking free curved beam element by choosing curvatures as nodal parameters instead of displacements, and by incorporating shear and membrane strains into the total potential energy by the force equilibrium equation.

Balasubramanian and Prathap (1989) developed a field consistent higher-order (wherein cubic polynomial was used for tangential, radial, as well as cross-sectional rotational degrees of freedom) curved beam element based on Timoshenko's theory for the analysis of stepped circular arches. Litewka and Rakowski (1998) employed analytical shape functions using algebraic-trigonometric functions to develop an exact stiffness matrix for studying curved beams with constant curvature.

Ganapathi et al. (1999) developed a cubic B-spline based field consistent element for the analysis laminated curved beams. Raveendranath et al. (2000) proposed a Timoshenko's theory based field consistent two-noded curved composite beam element, which incorporates flexural, axial, and shear loadings in the plane of the beam. Matsunaga (2003) reported a global higher-order arch theory by taking transverse shear and normal stress components into account. By expanding the displacements through power series, he derived the fundamental equilibrium equations through the principle of virtual work, for laminated circular arches.

Malekzadeh (2009) studied thick laminated composite circular arches under static loads using Differential Quadrature Method. Cevik (2007) analyzed a steel fiber reinforced aluminum metal-matrix laminated composite arch under thermal loads to explore the effects of lay up angle, number of layers, stacking

sequence, etc., on the residual stresses. Kim and Chaudhuri (2009) studied the large deflection behavior of symmetrically laminated thin shallow circular arch under a central concentrated load using Rayleigh–Ritz finite element method with C^1 continuity for the radial deformation and C^0 continuity for the tangential displacement.

A perusal of earlier works would reveal that the arch formulations for static loading conditions had been made either with classical theory or first-order shear deformable theory of Timoshenko. It is quite well known that the classical theory would be adequate only for thin sections. While first-order theory can handle relatively thick sections, it has serious limitations such as the need for a shear correction factor (Cowper 1966), inability to model the cross sectional warping—a key factor for sandwich constructions with stiff facings and weak cores. Also, it cannot model the variation of transverse displacement across the thickness, or in other words, the transverse normal strain.

Thus, the need for a theory capable of accurately modeling and analyzing deep composite and sandwich arches is quite evident. This paper presents a Higher-Order Arch Model (HOAM), precisely fulfilling that need.

The HOAM models the cross-sectional warping through a cubic axial strain; considers the variation of transverse displacement across the thickness through a linearly varying transverse normal strain; it also incorporates transverse shear strain, varying cubically across the cross section. This theory does not require any shear correction factor and employs standard isoparametric elements. Its elasticity matrix had been derived from an orthotropic lamina assumed to be in a three-dimensional state of stress, in such a way that even angle ply laminations can be studied using one-dimensional elements.

The HOAM is validated through the static analyses of shallow to deep and thin to thick laminated arches, with various boundary conditions. The role of curvature, aspect ratio, and end conditions on the transverse deformations of a sandwich and composite arch are investigated through parametric studies and suitable conclusions are drawn.

Theoretical Formulation

The Higher-Order Arch Model (HOAM), based on Taylor's series expansion (Lo et al. 1977), can be expressed, for an arch, as follows:

$$u = u_0 + z\theta_x + z^2 u_0^* + z^3 \theta_x^* \tag{1}$$

$$w = w_0 + z\theta_z + z^2 w_0^* \tag{2}$$

where z=distance from the neutral axis to any point of interest along the depth of the arch; u_0 and w_0=axial and transverse displacements in x-z plane; θ_x=face rotation about the y-axis, as shown in Fig. 1; and $u_0^*, \theta_x^*, \theta_z, w_0^*$=higher-order terms arising out of Taylor's series expansion and defined at the neutral axis.

The total potential energy of a system can be given as

$$\Pi = U - W \tag{3}$$

where U=internal strain energy; and W is the work done by the external forces. The same can be expressed as
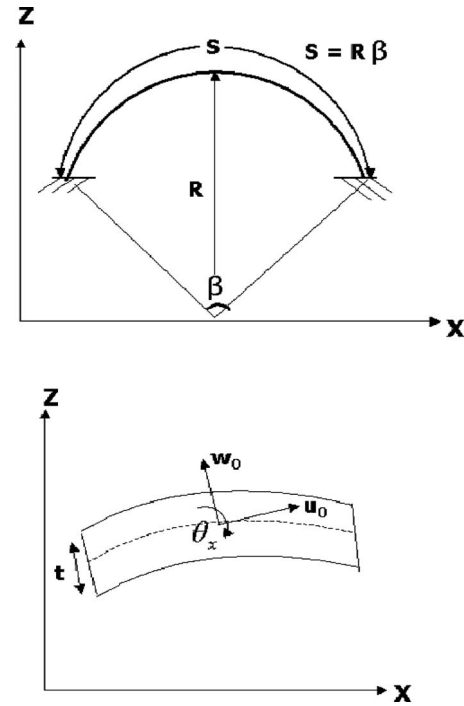
$$U = \frac{1}{2}\int \varepsilon^t \sigma \, dv \tag{4a}$$

Fig. 1. Arch geometry with displacement components

$$W = b \int \underset{\sim}{u}^t \underset{\sim}{p} \, dx \tag{4b}$$

where

$$\underset{\sim}{u} = [u \quad w]^t, \quad \varepsilon = [\varepsilon_x \quad \varepsilon_z \quad \gamma_{xz}]^t, \quad \sigma = [\sigma_x \quad \sigma_z \quad \tau_{xz}]^t,$$
$$\underset{\sim}{p} = [p_x \quad p_z]^t \tag{4c}$$

The field variables can be expressed in terms of nodal degrees of freedom as

$$\underset{\sim}{u} = Z_d d \tag{5a}$$

where

$$d = [u_0 \quad w_0 \quad \theta_x \quad u_0^* \quad \theta_x^* \quad \theta_z \quad w_0^*]^t \tag{5b}$$

$$Z_d = \begin{bmatrix} 1 & 0 & z & z^2 & z^3 & 0 & 0 \\ 0 & 1 & 0 & 0 & 0 & z & z^2 \end{bmatrix} \tag{5c}$$

The strain field for an arch (Qatu 2004) can be expressed as

$$\varepsilon_x = \frac{1}{(1 + z/R)}(u_{,x} + w/R) \tag{6a}$$

$$\varepsilon_z = w_{,z} \tag{6b}$$

$$\gamma_{xz} = w_{,x} + u_{,z} - u/R \tag{6c}$$

where R=radius of curvature.

Applying the displacement field from Eqs. (1) and (2) in the above equations, one gets

$$\varepsilon_x = \varepsilon_{x0} + z^2 \varepsilon_{x0}^* + z\kappa_x + z^3 \kappa_x^* \tag{7a}$$

$$\varepsilon_z = \varepsilon_{z0} + z\kappa_z \tag{7b}$$

$$\gamma_{xz} = \phi + z^2\phi^* + z\chi_{xz} + z^3\chi_{xz}^* \qquad (7c)$$

and can be expressed in matrix form as

$$\varepsilon_x = Z_a^t \varepsilon_a + Z_b^t \varepsilon_b \qquad (8)$$

$$\varepsilon_z = Z_t^t \varepsilon_t \qquad (9)$$

$$\gamma_{xz} = Z_s^t \gamma_s \qquad (10)$$

where

$$\varepsilon_a = [\varepsilon_{x0} \quad \varepsilon_{x0}^*]^t = [(u_{0,x} + w_0/R) \quad (u_{0,x}^* + w_0^*/R)]^t \qquad (11a)$$

$$\varepsilon_b = [\kappa_x \quad \kappa_x^*]^t = [(\theta_{x,x} + \theta_z/R) \quad (\theta_{x,x}^*)]^t \qquad (11b)$$

$$\varepsilon_t = [\varepsilon_{z0} \quad \kappa_z]^t = [\theta_z \quad 2w_0^*]^t \qquad (11c)$$

$$\gamma_s = [\phi \quad \phi^* \quad \chi_{xz} \quad \chi_{xz}^*]^t = [(w_{0,x} + \theta_x - u_0/R)$$
$$(w_{0,x}^* + 3\theta_x^* - u_0^*/R) \quad (\theta_{z,x} + 2u_0^* - \theta_x/R) \quad (-\theta_x^*/R)]^t$$
$$(11d)$$

$$Z_a = \left[\frac{1}{(1+z/R)} \quad \frac{z^2}{(1+z/R)}\right]^t \qquad (11e)$$

$$Z_b = \left[\frac{z}{(1+z/R)} \quad \frac{z^3}{(1+z/R)}\right]^t \qquad (11f)$$

$$Z_t = [1 \quad z]^t \qquad (11g)$$

$$Z_s = [1 \quad z^2 \quad z \quad z^3]^t \qquad (11h)$$

The strains of Eqs. (8)–(11) can be rewritten in a combined matrix form as

$$\varepsilon = \bar{Z}\bar{\varepsilon} \qquad (12a)$$

where

$$\bar{Z} = \begin{bmatrix} Z_a^t & Z_b^t & 0 & 0 \\ 0 & 0 & Z_t^t & 0 \\ 0 & 0 & 0 & Z_s^t \end{bmatrix} \qquad (12b)$$

$$\bar{\varepsilon} = [\varepsilon_a \quad \varepsilon_b \quad \varepsilon_t \quad \gamma_s]^t \qquad (12c)$$

The stress-strain relationship of an orthotropic lamina in a three-dimensional state of stress can be expressed as (Jones 1975)

$$\sigma^o = Q\varepsilon^o \qquad (13a)$$

where

$$\sigma^o = [\sigma_x \quad \sigma_y \quad \sigma_z \quad \tau_{xy} \quad \tau_{yz} \quad \tau_{xz}]^t \qquad (13b)$$

$$\varepsilon^o = [\varepsilon_x \quad \varepsilon_y \quad \varepsilon_z \quad \gamma_{xy} \quad \gamma_{yz} \quad \gamma_{xz}]^t \qquad (13c)$$

and Q is given by Eqs. (45)–(57) in Appendix I.

By setting $\sigma_y, \tau_{xy}, \tau_{yz}$ equal to zero in Eq. (13a) and deriving the remaining stress components from the same equation (Vinayak et al. 1996), one gets the stress strain relationship as

$$\sigma = C\varepsilon \qquad (14a)$$

where

$$\sigma = [\sigma_x \quad \sigma_z \quad \tau_{xz}]^t \qquad (14b)$$

$$C = \begin{bmatrix} C_{11} & C_{12} & 0 \\ C_{21} & C_{22} & 0 \\ 0 & 0 & C_{33} \end{bmatrix} \qquad (14c)$$

and the expressions for various C matrix elements are given by Eqs. (58)–(63) in Appendix II.

The internal strain energy can be evaluated using Eqs. (12a)–(12c) and (14a)–(14c) as

$$U = \frac{1}{2} \int \varepsilon^t \sigma dv = \frac{1}{2} \int \bar{\varepsilon}^t \bar{D}\bar{\varepsilon} dx \qquad (15a)$$

where

$$\bar{D} = b \int \bar{Z}^t C\bar{Z} dz \qquad (15b)$$

$$= b \int \begin{bmatrix} Z_a C_{11} Z_a^t & Z_a C_{11} Z_b^t & Z_a C_{12} Z_t^t & 0 \\ Z_b C_{11} Z_a^t & Z_b C_{11} Z_b^t & Z_b C_{12} Z_t^t & 0 \\ Z_t C_{21} Z_a^t & Z_t C_{21} Z_b^t & Z_t C_{22} Z_t^t & 0 \\ 0 & 0 & 0 & Z_s C_{33} Z_s^t \end{bmatrix} dz \qquad (15c)$$

$$= \begin{bmatrix} D_{aa} & D_{ab} & D_{at} & 0 \\ D_{ba} & D_{bb} & D_{bt} & 0 \\ D_{ta} & D_{tb} & D_{tt} & 0 \\ 0 & 0 & 0 & D_{ss} \end{bmatrix} \qquad (15d)$$

and the expansions of various D matrices are given by Eqs. (66)–(75), in Appendix III.

The external work done of Eq. (4b) can be modified with Eq. (5a) as

$$W = d^t \int \underset{\sim}{P} dx \qquad (16a)$$

where

$$\underset{\sim}{P} = bZ_d^t \underset{\sim}{p} \qquad (16b)$$

$$= b[p_x \quad p_z \quad zp_x \quad z^2 p_x \quad z^3 p_x \quad zp_z \quad z^2 p_z]^t \qquad (16c)$$

This vector can now be expressed as

$$\underset{\sim}{P} = [p_{x0} \quad p_{z0} \quad m_{x0} \quad p_{x0}^* \quad m_{x0}^* \quad m_{z0} \quad p_{z0}^*]^t \qquad (17)$$

Now, the total potential energy can be restated with Eqs. (15a) and (16a) as

$$\Pi = \frac{1}{2} \int (\bar{\varepsilon}^t \bar{D}\bar{\varepsilon}) dx - d^t \int \underset{\sim}{P} dx \qquad (18)$$

Finite-Element Modeling

The displacements within an element can be expressed in terms of its nodal displacements in isoparametric formulations as

$$d = Na_e \tag{19}$$

where N=shape function vector (Appendix IV); and a_e=vector containing nodal displacement vectors of an element with n nodes and can be expressed as

$$a_e = [d_1^t \quad d_2^t \quad \dots \quad d_n^t]^t \tag{20}$$

Similarly, the strains with in an element can be written through Eqs. (5b) and (12c) as

$$\bar{\varepsilon} = \begin{bmatrix} B_a \\ B_b \\ B_t \\ B_s \end{bmatrix} a_e = \bar{B}a_e \tag{21}$$

where, for a given node n, the strain displacement matrix can be computed as

$$B_a = \begin{bmatrix} N_{,x} & N/R & 0 & 0 & 0 & 0 & 0 \\ 0 & 0 & 0 & N_{,x} & 0 & 0 & N/R \end{bmatrix}_n \tag{22}$$

$$B_b = \begin{bmatrix} 0 & 0 & N_{,x} & 0 & 0 & N/R & 0 \\ 0 & 0 & 0 & 0 & N/R & 0 & 0 \end{bmatrix}_n \tag{23}$$

$$B_t = \begin{bmatrix} 0 & 0 & 0 & 0 & 0 & N & 0 \\ 0 & 0 & 0 & 0 & 0 & 0 & 2N \end{bmatrix}_n \tag{24}$$

$$B_s = \begin{bmatrix} -N/R & N_{,x} & N & 0 & 0 & 0 & 0 \\ 0 & 0 & 0 & -N/R & 3N & 0 & N_{,x} \\ 0 & 0 & -N/R & 2N & 0 & N_{,x} & 0 \\ 0 & 0 & 0 & 0 & -N/R & 0 & 0 \end{bmatrix}_n \tag{25}$$

By substituting Eqs. (19) and (21) in Eq. (18), one gets

$$\Pi = \tfrac{1}{2} a_e^t \int \bar{B}^t \bar{D} \bar{B} dx a_e - a_e^t \left[P_C + \int N^t \underset{\sim}{P} \, dx \right] \tag{26}$$

where P_C=vector of nodal concentrated loads of an element.

Minimizing the total potential energy of Eq. (26) with respect to nodal degrees of freedom, we get the static equilibrium equation as

$$Ka_e = F \tag{27a}$$

where

$$K = \int \bar{B}^t \bar{D} \bar{B} \, dx \tag{27b}$$

$$F = P_C + \int N^t \underset{\sim}{P} \, dx \tag{27c}$$

The external force vector of Eq. (27c) can be expressed as

$$F = P_C + \Sigma w_g N^t \underset{\sim}{P} |J| \tag{28a}$$

where

$$\underset{\sim}{P} = b \begin{bmatrix} 0 & p_z & 0 & 0 & 0 & \dfrac{t}{2} p_z & \dfrac{t^2}{4} p_z \end{bmatrix} \tag{28b}$$

and p_z can either be the uniformly distributed transverse load or the central amplitude of the sinusoidal load.

Assembling the stiffness and force vectors of all elements, given by Eq. (27a), one gets the global static equilibrium of the structure, which can be solved by using any standard solver for static equilibrium equations (Bathe 1982), after applying suitable boundary conditions, and the deformations of the structure can be estimated.

Numerical Experiments

Numerical experiments have been carried out to study the performance of the HOAM. This model is first validated by comparing its results with those available in the literature, and subsequently its performance has been carefully studied for various material and geometric conditions. Details such as material properties, lamination scheme and end conditions of every problem solved, are given in Table 1.

Validation Experiments

First, a standard beam problem is analyzed using HOAM. Results of a beam of length 10, Young's modulus of 1.05×10^7, v of 0.25, cross-section depth of 0.125 and width of 1.2, and applied load of 10 (both concentrated and uniformly distributed) are given in Table 2, where in HOAM can be seen to predict results quite close to analytical solutions of Gere and Weaver (1965).

A clamped-free (CF) arch with tip load (Fig. 2) and a pinched ring (PR) (Fig. 3) are analyzed with HOAM, and its results are presented in Table 3. One can observe close correlation with exact solutions and field consistent finite element results (Balasubramanian and Prathap 1989).

Next, a 90° circular ring under pure bending (Fig. 4) is studied and the normalized displacements with exact solutions for different R/t ratios are presented in Table 4. Also, a circular arch with central concentrated load (Fig. 5) is analyzed with HOAM. The predictions of HOAM are compared with exact results in Table 5. In both cases, the HOAM computes results quite closer to exact solutions.

A quarter ring with a radial load at the tip (Fig. 6) and a pinched ring (Fig. 3) solved by Lee and Sin (1994) are modeled with HOAM for various R/t and S/t ratios—from thin to thick arch cross sections—and the results normalized with analytical solutions are given in Tables 6 and 7. The results of HOAM agree very well with those of analytical solutions. However, the normalized deformations vary as the arch becomes thicker, primarily because the analytical solutions considered are based on first-order shear deformation theory (FOST) of Timoshenko (1921), which does not capture the cross-sectional warping of deeper cross sections as well as the transverse normal strains, while HOAM incorporates both of them.

Three arch problems [Figs. 7(a and b), Fig. 3] analyzed by Ganapathi et al. (1999) are studied by HOAM, and the results are shown in Table 8. Close correlation with the earlier studies can be observed in this problem as well. Next, a laminated arch sector subjected to sinusoidal load (Fig. 8) is studied for various R/t ratios, where the close correlation of HOAM results with the spline based element and elasticity solution can be observed (Table 9). The pinched ring (Fig. 3) of Kulikov and Plotnikova (2004) is modeled with HOAM and one can observe the perfect match between HOAM and this reference, for various R/t ratios, in Table 10.

Matsunaga's arch sector (2003) subjected to sinusoidal load

Table 1. Data for Numerical Experiments

	Boundary conditions for different supports	
Support type	at $x=0$	at $x=S$
Simply supported (SS)	$u_0=u_0^*=0$	$u_0=u_0^*=0$
	$w_0=\theta_z=w_0^*=0$	$w_0=\theta_z=w_0^*=0$
Roller-simply supported (RS)	—	$u_0=u_0^*=0$
	$w_0=\theta_z=w_0^*=0$	$w_0=\theta_z=w_0^*=0$
Clamped-clamped (CC)	$u_0=u_0^*=\theta_x=\theta_x^*=0$	$u_0=u_0^*=\theta_x=\theta_x^*=0$
	$w_0=\theta_z=w_0^*=0$	$w_0=\theta_z=w_0^*=0$
Clamped-free (CF)	$u_0=u_0^*=\theta_x=\theta_0^*=0$	All free
	$w_0=\theta_z=w_0^*=0$	—
Pinched-ring (PR)	$u_0=u_0^*=\theta_x=\theta_x^*=0$	$u_0=u_0^*=\theta_x=\theta_x^*=0$

No.	Material data details	Ref.
Data-1		(Balasubramanian and Prathap 1989)

Data-1a (Fig. 2)

$E_1=E_2=E_3=6.8948$ GPa $(1\times10^6$ lb/in.$^2)$

$G_{12}=G_{23}=G_{13}=2.6519$ GPa $(3.8462\times10^5$ lb/in.$^2)$

$R=254$ mm (10 in.)

$S=254$ mm (10 in.), $\beta=57.2958°$

$v=0.3$, $b=25.4$ mm (1 in.), $t=0.27823$ mm (0.010954 in.)

$P_C=0.048726$ N (0.010954 lb)

BC: CF

Data-1b (Fig. 3)

$E_1=E_2=E_3=72.395$ GPa $(1.05\times10^7$ lb/in.$^2)$

$G_{12}=G_{23}=G_{13}=47.5092$ GPa $(6.890625\times10^6$ lb/in.$^2)$

$R=125.81$ mm (4.953 in.)

S (of quarter ring)$=197.62$ mm (7.7802 in.), $\beta=90°$

$v=0.3125$, $b=25.4$ mm (1 in.), $t=2.3876$ mm (0.094 in.)

$P_C=444.82$ N (100 lb), Load on quarter ring$=222.41$ N (50 lb)

BC: PR

Data-2 (Fig. 4)		(Stolarski and Chiang 1989)

$E_1=E_2=E_3=72.395$ GPa $(1.05\times10^7$ lb/in.$^2)$

$G_{12}=G_{23}=G_{13}=28.958$ GPa $(4.2\times10^6$ lb/in.$^2)$

$\beta=90°$

$v=0.25$, $b=30.48$ mm (1.2 in.)

$M_0=0.11298$ N·m (1 lb·in.)

BC: CF

Exact values:

$$u=\frac{MR^2}{EI}\left(\frac{\Pi}{2}-1\right)$$

$$w=\frac{MR^2}{EI}$$

$$\theta=\frac{\Pi MR}{2EI}$$

Data-3 (Fig. 5)		(Stolarski and Chiang 1989)

$E_1=E_2=E_3=72.395$ GPa $(1.05\times10^7$ lb/in.$^2)$

$G_{12}=G_{23}=G_{13}=27.845$ GPa $(4.0385\times10^6$ lb/in.$^2)$

$\beta=315°$

$v=0.3$, $b=30.48$ mm (1.2 in.), $t=3.175$ mm (0.125 in.)

$R=74.549$ mm (2.935 in.), $S=409.85$ mm (16.136 in.)

$P_C=4.4482$ N (1 lb)

BC: CC

Table 1. (*Continued.*)

No.	Material data details	Ref.
Data-4		(Lee and Sin 1994)

Data-4 Data-4a (Fig. 6)

$E_1 = E_2 = E_3 = 72.395$ GPa (1.05×10^7 lb/in.^{2})

$G_{12} = G_{23} = G_{13} = 36.1975$ GPa (5.25×10^6 lb/in.^{2})

$\beta = 90°$

$v = 0$, $b = 25.4$ mm (1 in.)

$P_C = 222.41$ N (50 lb)

BC: CF

Analytical:

$u = PR^3/2EI - PR/2kGA - PR/2EA$

$w = \Pi PR^3/4EI + \Pi PR/4kGA + \Pi PR/4EA$

$\theta = PR^2/EI$

Data-4b (Fig. 3)

$P_C = 444.82$ N (100 lb), Load on quarter ring $= 222.41$ N (50 lb)

BC: PR

Rest are the same as Data-4a

Analytical:

$w_1 = (\Pi - 4)PR^3/2\Pi EI - PR/2kGA + PR/2EA$

$w_2 = (\Pi^2 - 8)PR^3/4\Pi EI + \Pi PR/4kGA + \Pi PR/4EA$

Data-5		(Ganapathi et al. 1999)

Data-5 Data-5a [Figs. 7(a and b)]

$E_1 = E_2 = E_3 = 82.73709$ KPa (12 lb/in.^{2})

$G_{12} = G_{23} = G_{13} = 33.09484$ KPa (4.8 lb/in.^{2})

$R = 2540$ mm (100 in.)

$S = 7979.6$ mm (314.1593 in.), $\beta = 180°$

$v = 0.25$, $b = 25.4$ mm (1 in.)

$P_C = 4.4482$ N (1 lb)

$S/t = 10,100$

BC: CC, CF

NDP: $w * EI/P_C R^3$

Data-5b (Fig. 3)

S (of quarter ring) $= 3989.8$ mm (157.0796 in.), $\beta = 90°$

$P_C = 4.4482$ N (1 lb), Load on quarter ring $= 2.2241$ N (0.5 lb)

BC: PR

NDP: $w * 2EI/P_C R^3$

Rest are the same as Data-5a

Data-6 (Fig. 8)		(Ganapathi et al. 1999)

$E_1 = 172.3689$ KPa (25 lb/in.^{2}), $E_2 = E_3 = 6.894757$ KPa (1 lb/in.^{2})

$G_{12} = 3.4474$ KPa (0.5 lb/in.^{2}), $G_{23} = 1.379$ KPa (0.2 lb/in.^{2})

$G_{13} = 3.4474$ KPa (0.5 lb/in.^{2})

$R = 2540$ mm (100 in.)

$S = 2659.9$ mm (104.7198 in.), $\beta = 60°$

$v = 0.25$, $b = 25.4$ mm (1 in.)

$P_S = 6.8948$ KPa (1 lb/in.^{2})

BC: RS

NDP: $w * 10E_1 t^3/P_S R^4$

Lamination: [0/90/0]

Data-7 (Fig. 3)		(Kulikov and Plotnikova 2004)

$E_1 = E_2 = E_3 = 68.9476$ GPa (1×10^7 lb/in.^{2})

$G_{12} = G_{23} = G_{13} = 44.816$ GPa (6.5×10^6 lb/in.^{2})

$R = 2540$ mm (100 in.)

$v = 0.3$, $b = 25.4$ mm (1 in.)

S (of quarter ring) $= 3989.8$ mm (157.0796 in.), $\beta = 90°$

Table 1. (*Continued.*)

No.	Material data details	Ref.
	$P_C=444.82$ N (100 lb), load on quarter ring=222.41 N (50 lb)	
	BC: PR	
	Exact: $w=0.8927 P_C R^3 / Et^3$	
Data-8 (Fig. 8)		(Matsunaga 2003)
	$E_1=144.8$ GPa, $E_2=E_3=9.65$ GPa	
	$G_{12}=4.14$ GPa, $G_{23}=3.45$ GPa, $G_{13}=3.45$ GPa	
	$S=100$ m	
	$v=0.3$, $b=1$ m	
	$P_S=1$ N/m^2	
	BC: RS	
	NDP: $w^*E_1 t^3 / P_S S^4$	
	Lamination: $[0/90]$, $[0/90/0]$	
Material data—sandwich		
	Face: Graphite/Epoxy	(Chen and Sun 1985)
	$E_x=120.11$ GPa $(0.1742 \times 10^8$ lb/in.$^2)$	
	$E_y=E_z=7.9083$ GPa $(0.1147 \times 10^7$ lb/in.$^2)$	
	$G_{xy}=G_{yz}=G_{xz}=5.5041$ GPa $(0.7983 \times 10^6$ lb/in.$^2)$	
	$kG_{xy}=kG_{yz}=kG_{xz}=4.5871$ GPa $(0.6653 \times 10^6$ lb/in.$^2)$	
	$v_f=0.3$	
	Core: Aluminium honeycomb (0.25 in. cell size, 0.007 in. foil)	(Allen 1969)
	$E_x=E_y=E_z=G_{xy}=v_c=0$	
	$G_{yz}=70.395$ MPa $(0.1021 \times 10^5$ lb/in.$^2)$	
	$G_{xz}=140.79$ MPa $(0.2042 \times 10^5$ lb/in.$^2)$	
	$kG_{yz}=58.661$ MPa $(0.8508 \times 10^4$ lb/in.$^2)$	
	$kG_{xz}=117.35$ MPa $(0.1702 \times 10^5$ lb/in.$^2)$	
	$t_c/t_f=8$	
Material data—composite		(Reddy 1982)
	$E_x=525.38$ GPa $(0.762 \times 10^8$ lb/in.$^2)$	
	$E_y=E_z=21.015$ GPa $(0.3048 \times 10^7$ lb/in.$^2)$	
	$G_{xy}=G_{yz}=G_{xz}=10.508$ GPa $(0.1524 \times 10^7$ lb/in.$^2)$	
	$kG_{xy}=kG_{yz}=kG_{xz}=8.7563$ GPa $(0.127 \times 10^7$ lb/in.$^2)$	
	$v=0.25$	
Data-9 (Fig. 6)		
Data-9a		
	Material data—composite	
	$\beta=90°$	
	$b=25.4$ mm (1 in.), $t=25.4$ mm (1 in.)	
	$P_C=222.41$ N (50 lb)	
	BC: CF	
	Lamination: $[30/-30/30]$	
Data-9b		
	Lamination: $[0/45/-45/90]$	
	Rest are the same as Data-9a	
Data-9c		
	Material data—sandwich	
	$\beta=90°$	
	$b=25.4$ mm (1 in.)	
	t_f (top,bot)$=2.54$ mm (0.1 in.), $t_c=20.32$ mm (0.8 in.)	
	$P_C=222.41$ N (50 lb)	
	BC: CF	
	Lamination: $[0/30/45/60/\text{core}/60/45/30/0]$	
Data-9d		
	Lamination: $[0/90/\text{core}/0/90]$	
	Rest are the same as Data-9c	

Table 1. (*Continued.*)

No.	Material data details	Ref.
Data-10 (Fig. 3)		
Data-10a		
	Material data—composite	
	$\beta = 90°$	
	$b = 25.4$ mm (1 in.), $t = 25.4$ mm (1 in.)	
	$P_C = 444.82$ N (100 lb), load on quarter ring = 222.41 N (50 lb)	
	BC: PR	
	Lamination: $[30/-30/30]$	
Data-10b		
	Lamination: $[0/45/-45/90]$	
	Rest are the same as Data-10a	
Data-10c		
	Material data—Sandwich	
	$\beta = 90°$	
	$b = 25.4$ mm (1 in.)	
	t_f (top, bot) = 2.54 mm (0.1 in.), $t_c = 20.32$ mm (0.8 in.)	
	$P_C = 444.82$ N (100 lb), load on quarter ring = 222.41 N (50 lb)	
	BC: PR	
	Lamination: $[0/30/45/60/core/60/45/30/0]$	
Data-10d		
	Lamination: $[0/90/core/0/90]$	
	Rest are the same as Data-10c	
Data-11 (Fig. 9)		
Data-11a		
	Material data—composite	
	$\beta = 180°$	
	$R = 2540$ mm (100 in.), $S = 7979.6$ mm (314.1593 in.)	
	$b = 25.4$ mm (1 in.), $S/t = 5$	
	$P_C = 222.41$ N (50 lb), $M_0 = 5.6492$ N·m (50 lb·in.)	
	$P_U = 8.7563$ KN/m (50 lb/in.), $P_S = 344.74$ KPa (50 lb/in.^{2})	
	Lamination: $[30/-30/30]$	
Data-11b		
	Lamination: $[0/45/-45/90]$	
	Rest are the same as Data-11a	
Data-11c		
	Material data—sandwich	
	$\beta = 180°$	
	$R = 2540$ mm (100 in.), $S = 7979.6$ mm (314.1593 in.)	
	$b = 25.4$ mm (1 in.), $S/t = 5$	
	t_f (top, bot) = 159.59 mm (6.2832 in.), $t_c = 1276.7$ mm (50.2655 in.)	
	$P_C = 222.41$ N (50 lb), $M_0 = 5.6492$ N·m (50 lb·in.)	
	$P_U = 8.7563$ KN/m (50 lb/in.), $P_S = 344.74$ KPa (50 lb/in.^{2})	
	Lamination: $[0/30/45/60/core/60/45/30/0]$	
Data-11d		
	Lamination: $[0/90/core/0/90]$	
	Rest are the same as Data-11c	

(Fig. 8) is modeled with HOAM for symmetric and unsymmetric lamination schemes as in Table 11. The HOAM quite marginally underpredicts for unsymmetric laminates and over predicts for the symmetric laminates, compared to Matsunaga's formulation.

These examples have been carefully chosen in order to capture the variation in curvature, aspect ratio, and end conditions, on the response of the arch to static loads. The accuracy and adequacy of HOAM are validated through the good agreement observed be-tween the HOAM and the earlier works, which were reported in the literature.

HOAM Experiments

Now, different arch configurations such as quarter ring, pinched ring, and a circular arch are studied using HOAM for different laminations, loading, and end conditions.

Table 2. Performance Evaluation of a Beam with HOAM

Beam type	Loading	Response	Analytical (Gere and Weaver 1965)	HOAM	HOAM/ analytical
Simply supported	Uniformly distributed	Deflection	6.3492×10^{-1}	0.6351	1.0003
		Rotation	2.0317×10^{-1}	0.2031	0.9996
	Point load at center	Deflection	1.0159×10^{-1}	0.1016	1.0001
		Rotation	3.0476×10^{-2}	0.0305	0.9998
Cantilever	Point load at free end	Deflection	1.6254×10^{0}	1.6240	0.9991

First, a clamped-free arch with a tip load (Fig. 6) is studied for various lamination schemes and aspect ratios, and the results are presented in Table 12. In the case of symmetric and unsymmetric composites, HOAM is more flexible compared to FOST. Similarly, u_0 and w_0 predictions of HOAM for sandwich arches, are higher (twice or more for deeper sections) than those of
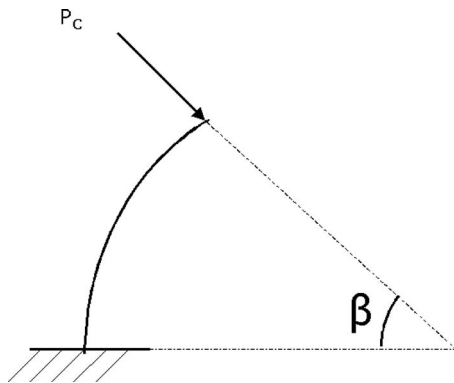
Fig. 2. Clamped-free arch segment with a radial tip load
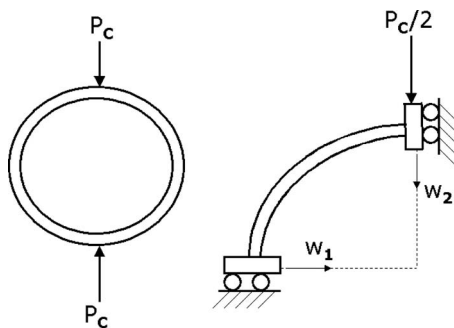
Fig. 3. Pinched ring and its quarter symmetry model

FOST; however, the θ_x of HOAM is lower than that of FOST. The unsymmetric configuration, for both composite and sandwich arches, is stiffer compared to its symmetric counterpart, for this problem.

Next, a laminated pinched ring (Fig. 3) is analyzed for various aspect ratios and the transverse displacements at the point of loading are given in Table 13. The HOAM is flexible for unsymmetric composites and sandwiches compared to FOST. While HOAM is stiffer for symmetric composites with the given angle ply lay up, it becomes flexible as the lamination tends towards cross-ply configuration. Also, the order of difference is quite significant in the case of sandwiches—HOAM results are more than thrice of FOST.

Transverse deformations at the central loading point of a deep circular arch (Fig. 9) with four types of load cases and end conditions are analyzed using HOAM and compared with those of FOST in Table 14. As one can observe, the HOAM is flexible compared to FOST and particularly for sandwiches, the order of difference is quite substantial. In the case of symmetric composites with simply supported (SS) and clamped-clamped (CC) end conditions, HOAM predicts stiffer results for the given angle ply lay up and becomes flexible as the lamination tends towards cross-ply configuration. Similarly, for clamped-free (CF) sandwich arches with central moment, we find HOAM to be stiffer than FOST; however, as the location of application of moment moves either towards the free end or the simply supported end, HOAM becomes flexible compared to FOST. On comparing the symmetric and unsymmetric laminates, one finds the unsymmetric laminates to be stiffer. However, in the case of higher-order composite arches with roller-simply supported (RS) end condition, symmetric laminates are stiffer.

The HOAM results of a circular arch under different types of loading, laminations, and boundary conditions are given in Table 15. The CC end condition produces stiffer arch than SS end condition. RS end condition produces perhaps the most flexible system followed by CF condition.

Table 3. Tip and Central Deflections (Data-1)

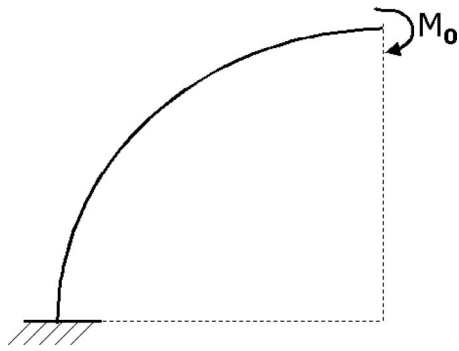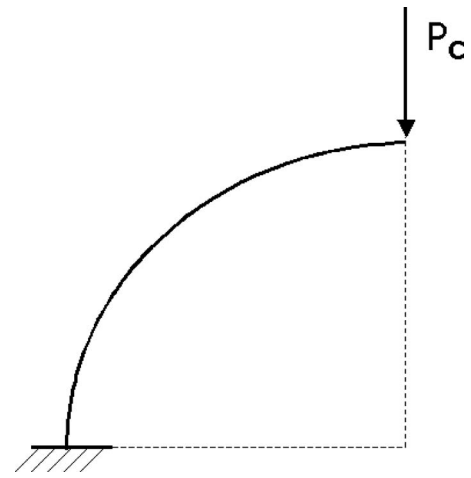| Source	Tip deflection of a clamped-free arch (Data-1a)	Source	Central deflection of a pinched ring (Data-1b)
Exact (Kikuchi and Tanizawa 1984)	27.2676	Babu and Prathap (1986)	1.2438
Balasubramanian and Prathap (1989)	27.2676	Balasubramanian and Prathap (1989)	1.2447
HOAM	27.2586	HOAM	1.24422

Fig. 4. Quarter ring with end moment

Fig. 6. Quarter ring with a radial load at tip

Table 4. Normalized Free end Displacements of a Cantilever Arch under Pure Bending (Data-2)

	HOAM/exact (Stolarski and Chiang 1989)		
R/t	u	w	θ
50	1.0000	0.9998	1.0127
100	0.9999	0.9999	1.0064
500	1.0001	1.0000	1.0012
1000	1.0001	0.9999	1.0005
10000	1.0000	0.9999	1.0000
100000	0.9996	0.9993	0.9994

Table 6. Normalized Tip Deformations of a Quarter Ring (Data-4a)

Aspect ratio		HOAM/analytical (Lee and Sin 1994)		
R/t	S/t	u	w	θ
100,000	50000 pi	0.9931	0.9937	0.9944
10,000	5000 pi	0.9999	0.9998	1.0000
1,000	500 pi	1.0000	1.0000	1.0000
200	100 pi	1.0000	1.0000	1.0000
100	50 pi	1.0000	1.0000	1.0000
20	10 pi	1.0011	0.9995	0.9998
10	5 pi	1.0043	0.9979	0.9992
5	2.5 pi	1.0175	0.9916	0.9967
3.333	1.667 pi	1.0401	0.9817	0.9930
2.5	1.25 pi	1.0743	0.9699	0.9892
2	pi	1.1217	0.9568	0.9860
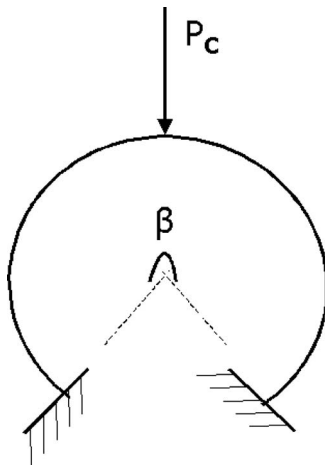
Fig. 5. Clamped-clamped arch with central load

Table 5. Central Deflection of a Circular Arch under Concentrated Force (Data-3)

Source	Vertical displacement at loading point
Stolarski and Belytschko (1983)	0.001061
Stolarski and Chiang (1989)	0.001061
HOAM	0.001062

Table 7. Normalized Tip Deformations of a Pinched Ring (Data-4b)

Aspect ratio		HOAM/analytical (Lee and Sin 1994)	
R/t	S/t	w_1	w_2
1,000,000	500000 pi	0.9783	0.9846
100,000	50000 pi	0.9973	0.9973
10,000	5000 pi	0.9995	0.9994
1,000	500 pi	1.0000	1.0000
200	100 pi	1.0000	1.0000
100	50 pi	1.0000	1.0000
20	10 pi	0.9995	0.9995
10	5 pi	0.9979	0.9979
5	2.5 pi	0.9918	0.9924
3.333	1.667 pi	0.9825	0.9844
2.5	1.25 pi	0.9720	0.9760
2	pi	0.9613	0.9679

Fig. 7. (a) Circular clamped-clamped arch with central load. (b) Circular clamped-free arch with tip load

Table 8. Normalized Transverse Deformations at the Loading Points (Data-5a, 5b)

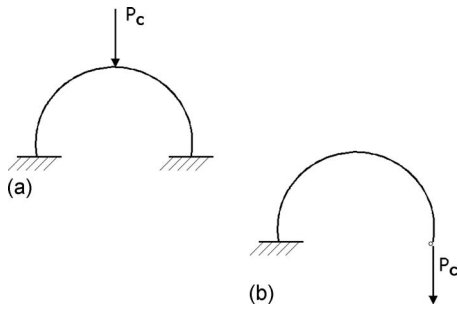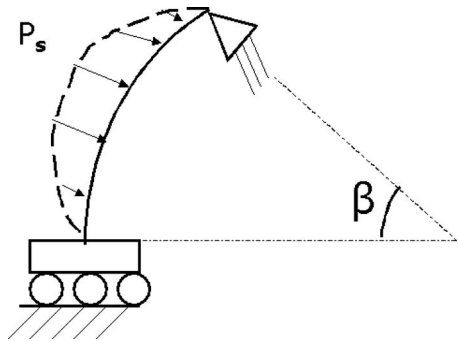| S/t	HOAM	Ganapathi et al. (1999)
Clamped-clamped circular arch		
10	0.026825	0.026860
100	0.011747	0.011800
1000000	0.011593	0.011590
Clamped-free circular arch		
10	1.585010	1.623590
100	1.570180	1.571300
1000000	1.413940	1.435370
Pinched ring		
10	0.154460	0.155390
100	0.148747	0.148840
1000000	0.150752	0.149420

Fig. 8. Arch segment with sinusoidal load

Table 9. Normalized Transverse Central Deformations of a Laminated Arch (Data-6)

R/t	HOAM	Ganapathi et al. (1999)	Elasticity [Ganapathi et al. (1999)]
20	2.2741	2.3767	2.38
50	1.9961	2.0245	2.02
100	1.9597	1.9690	1.96
1000	1.9466	1.9452	—
10000	1.9465	1.9442	—

Table 10. Normalized Transverse Deformations at the Loading Point of a Pinched Ring (Data-7)

R/t	HOAM/analytical (Kulikov and Plotnikova 2004)
100	0.9995
500	0.9994
1000	0.9994
10000	0.9994
100000	0.9973
1000000	0.9706

Table 11. Normalized Transverse Deformations of a Laminated Arch (Data-8)

S/t	S/R	HOAM	Matsunaga (2003)
	0/90		
5	0.5	0.7675	0.7829
	1	0.8892	0.9768
10	0.5	0.6181	0.6338
	1	0.7200	0.7612
	0/90/0		
5	0.5	0.3392	0.3292
	1	0.4004	0.3965
10	0.5	0.1866	0.1834
	1	0.2202	0.2178

Parametric Studies

In order to study the influence of curvature, aspect ratio, and end conditions on the deformations, a circular arch with a central concentrated load (P_C) with Data-11c for symmetric sandwich and Data-11b for unsymmetric composite lamination, is taken up.

The transverse deformations at the center of a sandwich circular arch, where the concentrated load is applied for various S/t ratios, are shown in Figs. 10–14. The CC end condition is the stiffest, followed by SS and CF, as one would expect. The arch with CC and SS end conditions demonstrates a similar response pattern: it becomes stiffer with the increase in internal angle up to 180° and thereafter becomes softer, for the same applied load. In the case of CF end condition, the structure becomes stiffer with the increase in internal angle.
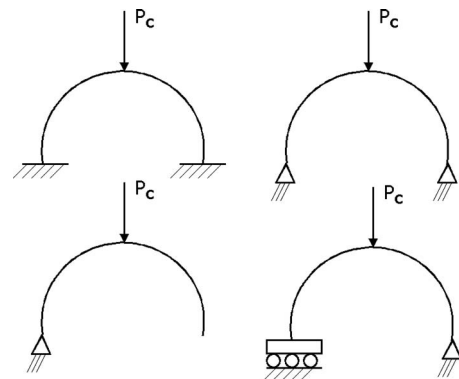

Fig. 9. Circular arch with various end and load conditions

Table 12. Deformations at the Loading Point of a Quarter Ring (Data-9)

Aspect ratio		u		w		θ		
R/t	S/t	HOAM	FOST	HOAM	FOST	HOAM	FOST	Data
2	pi	-4.0326×10^{-4}	-3.6457×10^{-4}	6.2240×10^{-4}	5.5583×10^{-4}	-3.5914×10^{-4}	-3.1984×10^{-4}	Sym comp: Data-9a
2.5	1.25 pi	-7.5596×10^{-4}	-6.9382×10^{-4}	1.1726×10^{-3}	1.0686×10^{-3}	-5.6018×10^{-4}	-5.1027×10^{-4}	
3.3333	1.667 pi	-1.7345×10^{-3}	-1.6125×10^{-3}	2.7035×10^{-3}	2.5044×10^{-3}	-9.9583×10^{-4}	-9.2270×10^{-4}	
5	2.5 pi	-5.7203×10^{-3}	-5.3684×10^{-3}	8.9517×10^{-3}	8.3895×10^{-3}	-2.2428×10^{-3}	-2.1025×10^{-3}	
10	5 pi	-4.5118×10^{-2}	-4.2602×10^{-2}	7.0802×10^{-2}	6.6832×10^{-2}	-8.9782×10^{-3}	-8.4754×10^{-3}	
2	pi	-3.6748×10^{-4}	-2.7387×10^{-4}	4.5872×10^{-4}	3.2578×10^{-4}	-2.9762×10^{-4}	-2.0126×10^{-4}	Unsym comp: Data-9b
2.5	1.25 pi	-6.5999×10^{-4}	-5.0964×10^{-4}	8.4649×10^{-4}	6.3301×10^{-4}	-4.4720×10^{-4}	-3.2568×10^{-4}	
3.3333	1.667 pi	-1.4461×10^{-3}	-1.1563×10^{-3}	1.9264×10^{-3}	1.5122×10^{-3}	-7.6917×10^{-4}	-5.9633×10^{-4}	
5	2.5 pi	-4.5392×10^{-3}	-3.7545×10^{-3}	6.3432×10^{-3}	5.2033×10^{-3}	-1.6828×10^{-3}	-1.3740×10^{-3}	
10	5 pi	-3.4017×10^{-2}	-2.9059×10^{-2}	5.0269×10^{-2}	4.2846×10^{-2}	-6.5697×10^{-3}	-5.5942×10^{-3}	
2	pi	-2.5356×10^{-3}	-1.0206×10^{-3}	3.9505×10^{-3}	1.4977×10^{-3}	-1.8764×10^{-4}	-6.4611×10^{-4}	Sym sandwich: Data-9c
2.5	1.25 pi	-3.7000×10^{-3}	-1.7488×10^{-3}	5.7509×10^{-3}	2.6145×10^{-3}	-6.0264×10^{-4}	-1.0244×10^{-3}	
3.3333	1.667 pi	-6.4444×10^{-3}	-3.7026×10^{-3}	1.0015×10^{-2}	5.6380×10^{-3}	-1.5014×10^{-3}	-1.8467×10^{-3}	
5	2.5 pi	-1.6103×10^{-2}	-1.1444×10^{-2}	2.5096×10^{-2}	1.7707×10^{-2}	-4.0692×10^{-3}	-4.2025×10^{-3}	
10	5 pi	-1.0153×10^{-1}	-8.6543×10^{-2}	1.5902×10^{-1}	1.3540×10^{-1}	-1.7924×10^{-2}	-1.6933×10^{-2}	
2	pi	-2.4924×10^{-3}	-8.2033×10^{-4}	3.8768×10^{-3}	1.2052×10^{-3}	6.9556×10^{-6}	-4.5291×10^{-4}	Unsym sandwich: Data-9d
2.5	1.25 pi	-3.5078×10^{-3}	-1.3644×10^{-3}	5.4396×10^{-3}	2.0323×10^{-3}	-2.9095×10^{-4}	-7.2236×10^{-4}	
3.3333	1.667 pi	-5.7748×10^{-3}	-2.8010×10^{-3}	8.9455×10^{-3}	4.2385×10^{-3}	-9.3525×10^{-4}	-1.3089×10^{-3}	
5	2.5 pi	-1.3302×10^{-2}	-8.4255×10^{-3}	2.0644×10^{-2}	1.2955×10^{-2}	-2.7761×10^{-3}	-2.9937×10^{-3}	
10	5 pi	-7.6437×10^{-2}	-6.2586×10^{-2}	1.1930×10^{-1}	9.7539×10^{-2}	-1.2716×10^{-2}	-1.2127×10^{-2}	

Table 13. Transverse Deformations at the Loading Point of a Pinched Ring (Data-10)

Aspect ratio		w		
R/t	S/t	HOAM	FOST	Data
2	pi	1.7930×10^{-4}	1.7991×10^{-4}	Sym comp: Data-10a
2.5	1.25pi	2.9888×10^{-4}	3.0712×10^{-4}	
3.3333	1.667pi	6.1430×10^{-4}	6.4659×10^{-4}	
5	2.5pi	1.8490×10^{-3}	1.9868×10^{-3}	
10	5pi	1.3718×10^{-2}	1.4957×10^{-2}	
2	pi	1.4146×10^{-4}	1.1925×10^{-4}	Unsym comp: Data-10b
2.5	1.25pi	2.2827×10^{-4}	1.9657×10^{-4}	
3.3333	1.667pi	4.5525×10^{-4}	4.0221×10^{-4}	
5	2.5pi	1.3371×10^{-3}	1.2172×10^{-3}	
10	5pi	9.7959×10^{-3}	9.2064×10^{-3}	
2	Pi	2.7631×10^{-3}	7.7831×10^{-4}	Sym sandwich: Data-10c
2.5	1.25pi	3.6418×10^{-3}	1.1275×10^{-3}	
3.3333	1.667pi	5.3410×10^{-3}	1.9459×10^{-3}	
5	2.5pi	9.9738×10^{-3}	4.8106×10^{-3}	
10	5pi	4.0653×10^{-2}	3.0029×10^{-2}	
2	Pi	2.9016×10^{-3}	6.9786×10^{-4}	Unsym sandwich: Data-10d
2.5	1.25pi	3.7919×10^{-3}	9.7924×10^{-4}	
3.3333	1.667pi	5.4406×10^{-3}	1.6131×10^{-3}	
5	2.5pi	9.6179×10^{-3}	3.7399×10^{-3}	
10	5pi	3.4171×10^{-2}	2.1789×10^{-2}	

Table 14. Transverse Deformations at the Center of a Circular Arch (Data-11)

Load type	SS HOAM	SS FOST	CC HOAM	CC FOST	CF HOAM	CF FOST	RS HOAM	RS FOST	Data
Concen	3.1104×10^{-5}	3.1541×10^{-5}	3.0939×10^{-5}	3.1518×10^{-5}	3.3173×10^{-4}	2.3831×10^{-4}	1.1038×10^{-2}	6.7106×10^{-4}	Sym comp:
Moment	0	0	0	0	-3.6000×10^{-6}	-2.2566×10^{-6}	1.0829×10^{-4}	6.2116×10^{-6}	Data-11a
udl	1.7611×10^{-3}	2.1041×10^{-3}	1.7584×10^{-3}	2.0635×10^{-3}	6.9888×10^{-2}	4.3663×10^{-2}	2.1969×10^{0}	1.3001×10^{-1}	
Sinusoidal	1.9252×10^{-3}	2.2393×10^{-3}	1.9107×10^{-3}	2.2164×10^{-3}	5.2125×10^{-2}	3.4549×10^{-2}	1.7284×10^{0}	1.0270×10^{-1}	
Concen	2.4474×10^{-5}	2.1611×10^{-5}	2.2627×10^{-5}	1.9431×10^{-5}	2.5111×10^{-4}	1.48×10^{-4}	1.2944×10^{-2}	6.5456×10^{-4}	Unsym comp:
Moment	0	0	0	0	-3.0652×10^{-6}	-1.4881×10^{-6}	1.2727×10^{-4}	6.0918×10^{-6}	Data-11b
udl	1.1832×10^{-3}	1.0466×10^{-3}	6.7964×10^{-4}	3.8720×10^{-4}	5.1823×10^{-2}	2.5570×10^{-2}	2.5745×10^{0}	1.2764×10^{-1}	
Sinusoidal	1.3435×10^{-3}	1.2286×10^{-3}	9.6557×10^{-4}	7.6613×10^{-4}	3.8906×10^{-2}	2.0588×10^{-2}	2.0263×10^{0}	1.0065×10^{-1}	
Concen	6.3309×10^{-4}	1.9224×10^{-4}	5.9101×10^{-4}	1.8276×10^{-4}	2.7268×10^{-3}	8.2239×10^{-4}	3.4389×10^{-1}	2.7392×10^{-3}	Sym sandwich:
Moment	0	0	0	0	-3.3361×10^{-6}	-5.1568×10^{-6}	3.2673×10^{-3}	2.3267×10^{-5}	Data-11c
udl	1.1098×10^{-2}	1.1094×10^{-2}	1.0329×10^{-2}	8.4665×10^{-3}	3.8653×10^{-1}	1.2750×10^{-1}	6.8584×10^{1}	5.2048×10^{-1}	
Sinusoidal	2.2829×10^{-2}	1.2209×10^{-2}	1.9982×10^{-2}	1.0327×10^{-2}	3.3603×10^{-1}	1.0686×10^{-1}	5.3943×10^{1}	4.1229×10^{-1}	
Concen	6.2929×10^{-4}	1.6822×10^{-4}	6.0239×10^{-4}	1.6218×10^{-4}	2.7369×10^{-3}	7.0990×10^{-4}	3.3217×10^{-1}	2.7061×10^{-3}	Unsym sandwich:
Moment	0	0	0	0	-1.5318×10^{-6}	-3.7954×10^{-6}	3.1734×10^{-3}	2.3214×10^{-5}	Data-11d
udl	5.7458×10^{-3}	6.9654×10^{-3}	7.1689×10^{-3}	5.3043×10^{-3}	3.6859×10^{-1}	1.0448×10^{-1}	6.6234×10^{1}	5.1454×10^{-1}	
Sinusoidal	1.8892×10^{-2}	8.8569×10^{-3}	1.8050×10^{-2}	7.6643×10^{-3}	3.2804×10^{-1}	8.9299×10^{-2}	5.2094×10^{1}	4.0751×10^{-1}	

Table 15. Deformations at the Center of a Circular Arch (Data-11)

Load type and BC	Sym Comp: Data-11a u	Sym Comp: Data-11a w	Sym Comp: Data-11a θ	Unsym Comp: Data-11b u	Unsym Comp: Data-11b w	Unsym Comp: Data-11b θ
SS-Con	0	3.1104×10^{-5}	0	0	2.4474×10^{-5}	0
SS-Mom	4.0026×10^{-9}	0	2.2996×10^{-8}	1.6022×10^{-7}	0	2.2100×10^{-8}
SS-udl	0	1.7611×10^{-3}	0	0	1.1832×10^{-3}	0
SS-Sin	-1.3683×10^{-9}	1.9252×10^{-3}	0	0	1.3435×10^{-3}	0
CC-Con	0	3.0939×10^{-5}	0	0	2.2627×10^{-5}	0
CC-Mom	4.7492×10^{-8}	0	2.2886×10^{-8}	1.9839×10^{-7}	0.0000×10^{0}	2.1421×10^{-8}
CC-udl	0	1.7584×10^{-3}	0	0	6.7964×10^{-4}	0
CC-Sin	0	1.9107×10^{-3}	0	0	9.6557×10^{-4}	0
CF-Con	-2.1729×10^{-4}	3.3173×10^{-4}	-3.6000×10^{-6}	-2.0812×10^{-4}	2.5111×10^{-4}	-3.0652×10^{-6}
CF-Mom	2.4035×10^{-6}	-3.6000×10^{-6}	7.2193×10^{-8}	2.8516×10^{-6}	-3.0652×10^{-6}	6.9495×10^{-8}
CF-udl	-4.3966×10^{-2}	6.9888×10^{-2}	-9.4740×10^{-4}	-4.4127×10^{-2}	5.1823×10^{-2}	-8.1133×10^{-4}
CF-Sin	-3.4043×10^{-2}	5.2125×10^{-2}	-6.5574×10^{-4}	-3.3491×10^{-2}	3.8906×10^{-2}	-5.6168×10^{-4}
RS-Con	1.0753×10^{-2}	1.1038×10^{-2}	1.0830×10^{-4}	1.2629×10^{-2}	1.2944×10^{-2}	1.2727×10^{-4}
RS-Mom	1.0580×10^{-4}	1.0829×10^{-4}	1.0885×10^{-6}	1.2457×10^{-4}	1.2727×10^{-4}	1.2760×10^{-6}
RS-udl	2.1444×10^{0}	2.1969×10^{0}	2.1598×10^{-2}	2.5154×10^{0}	2.5745×10^{0}	2.5351×10^{-2}
RS-Sin	1.6866×10^{0}	1.7284×10^{0}	1.6987×10^{-2}	1.9794×10^{0}	2.0263×10^{0}	1.9949×10^{-2}

| Load type and BC	Sym. Sandwich: Data-11c u	Sym. Sandwich: Data-11c w	Sym. Sandwich: Data-11c θ	Unsym. Sandwich: Data-11d u	Unsym. Sandwich: Data-11d w	Unsym. Sandwich: Data-11d θ
SS-Con	0	6.3309×10^{-4}	0	0	6.2929×10^{-4}	0
SS-Mom	1.3894×10^{-5}	0	8.0188×10^{-7}	1.0482×10^{-5}	0	6.2327×10^{-7}
SS-udl	-2.1359×10^{-9}	1.1098×10^{-2}	0	0	5.7458×10^{-3}	0
SS-Sin	-2.4615×10^{-8}	2.2829×10^{-2}	0	-2.3732×10^{-8}	1.8892×10^{-2}	0
CC-Con	0	5.9101×10^{-4}	0	0	6.0239×10^{-4}	0
CC-Mom	9.5138×10^{-6}	0.0000×10^{0}	6.3862×10^{-7}	5.9565×10^{-6}	0	4.4017×10^{-7}
CC-udl	-2.0325×10^{-9}	1.0329×10^{-2}	0	-1.3857×10^{-9}	7.1689×10^{-3}	0
CC-Sin	-1.8368×10^{-8}	1.9982×10^{-2}	0	-1.8247×10^{-8}	1.8050×10^{-2}	0
CF-Con	-1.7987×10^{-3}	2.7268×10^{-3}	-3.3361×10^{-6}	-1.8129×10^{-3}	2.7369×10^{-3}	-1.5318×10^{-6}
CF-Mom	1.2123×10^{-5}	-3.3361×10^{-6}	7.3287×10^{-7}	7.1661×10^{-6}	-1.5318×10^{-6}	5.1689×10^{-7}
CF-udl	-2.5211×10^{-1}	3.8653×10^{-1}	-1.4621×10^{-3}	-2.4085×10^{-1}	3.6859×10^{-1}	-9.6896×10^{-4}
CF-Sin	-2.3940×10^{-1}	3.3603×10^{-1}	-8.7745×10^{-4}	-2.3587×10^{-1}	3.2804×10^{-1}	-5.4134×10^{-4}
RS-Con	3.2795×10^{-1}	3.4389×10^{-1}	3.2673×10^{-3}	3.1857×10^{-1}	3.3217×10^{-1}	3.1734×10^{-3}
RS-Mom	3.1355×10^{-3}	3.2673×10^{-3}	3.1902×10^{-5}	3.0597×10^{-3}	3.1734×10^{-3}	3.0998×10^{-5}
RS-udl	6.5516×10^{1}	6.8584×10^{1}	6.5271×10^{-1}	6.3637×10^{1}	6.6234×10^{1}	6.3391×10^{-1}
RS-Sin	5.1516×10^{1}	5.3943×10^{1}	5.1324×10^{-1}	5.0038×10^{1}	5.2094×10^{1}	4.9845×10^{-1}
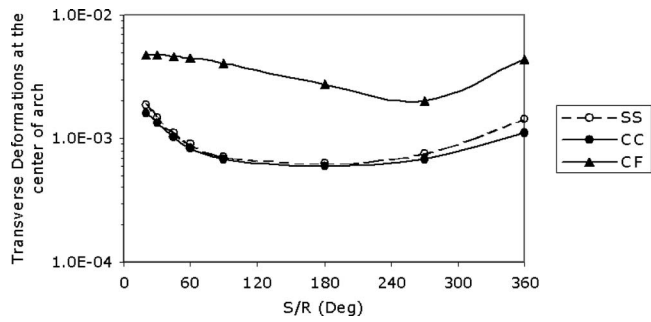
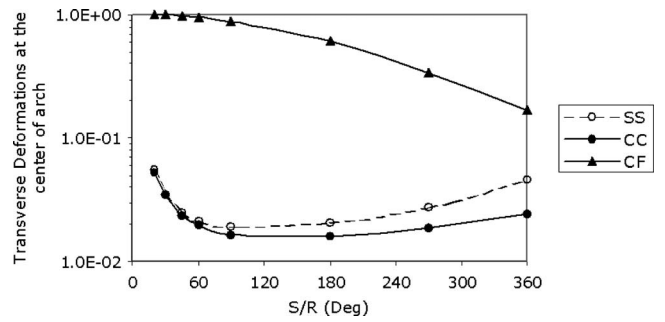**Fig. 10.** Sandwich arch with concen. load—S/t=5 (Data-11c)

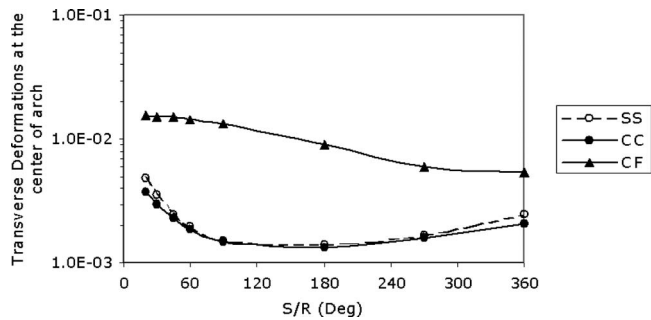**Fig. 14.** Sandwich arch with concen. load—S/t=50 (Data-11c)

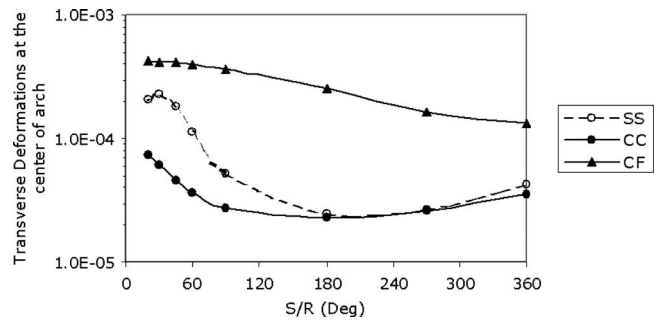**Fig. 11.** Sandwich arch with concen. load—S/t=10 (Data-11c)

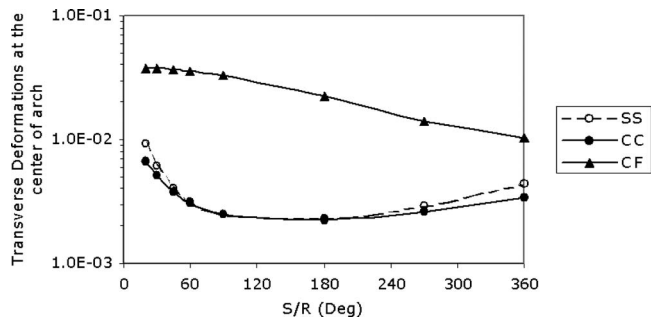**Fig. 15.** Composite arch with concen. load—S/t=5 (Data-11b)

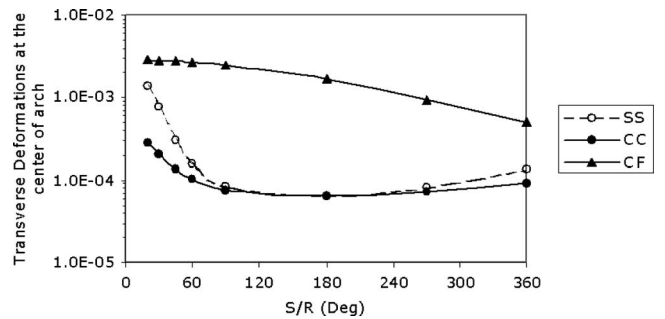**Fig. 12.** Sandwich arch with concen. load—S/t=15 (Data-11c)

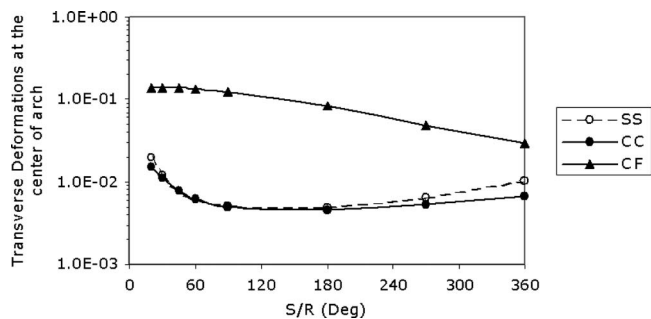**Fig. 16.** Composite arch with concen. load—S/t=10 (Data-11b)

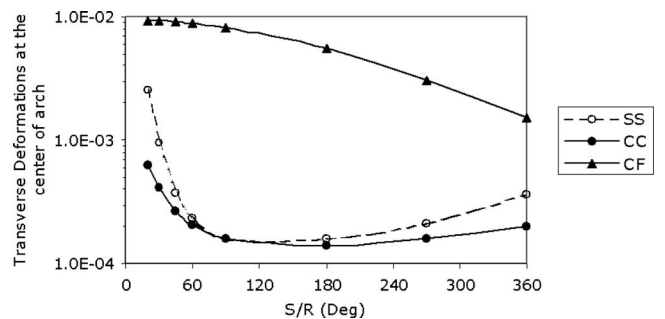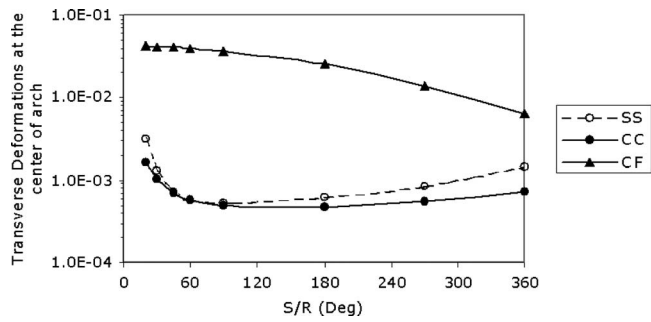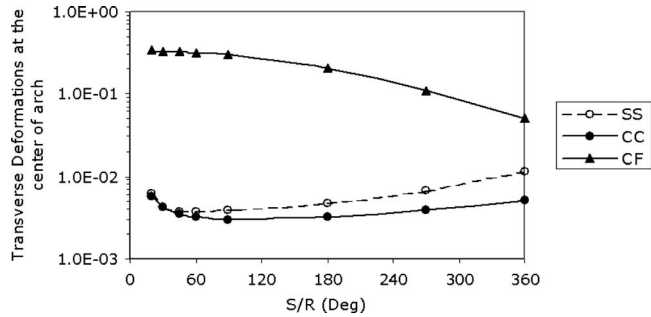**Fig. 13.** Sandwich arch with concen. load—S/t=25 (Data-11c)

Fig. 17. Composite arch with concen. load—S/t=15 (Data-11b)

Fig. 18. Composite arch with concen. load—$S/t=25$ (Data-11b)

Fig. 19. Composite arch with concen. load—$S/t=50$ (Data-11b)

The responses of an unsymmetric composite arch are presented in Figs. 15–19. The arch with SS end condition turns stiff quite steeply with the increase in the subtended angle. This internal angle at which the transition happens also changes with aspect ratio. The CC arch, which is the stiffest, also follows a similar pattern. The CF arch becomes stiffer with the increase in internal angle.

Conclusions

A higher-order arch model (HOAM) with transverse shear and normal strain components is formulated for studying the re-
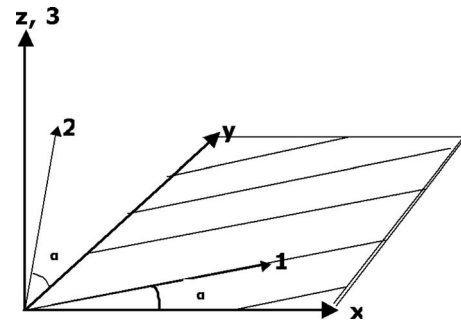
Fig. 20. Axis system—1,2,3: Lamina axes; x,y,z: laminate axes

sponse of laminated arches under various static loading conditions. The HOAM can study shallow to deep and thin to thick arch geometries quite effectively. Through the constitutive relationship, adapted from the three-dimensional stress-strain relationship of an orthotropic lamina, even angle-ply laminates can be analyzed using one-dimensional elements. The HOAM is validated through the results of earlier investigations. Subsequently, the response of HOAM for various materials, loading, boundary, and geometric conditions are presented and also compared with those of first-order shear deformation theory (FOST) of Timoshenko. Parametric studies on symmetric sandwich and unsymmetric composite arches have been carried out to study the role of curvature, aspect ratio, and end conditions on the transverse deformations.

Appendix I. Coefficients of *Q*-Matrix

The stress-strain relationship at a point of an orthotropic lamina in a three dimensional state of stress/ strain can be expressed (Jones 1975), along the lamina axes (Fig. 20) as

$$\sigma' = D\varepsilon' \tag{29}$$

where

$$\sigma' = \begin{bmatrix} \sigma_1 & \sigma_2 & \sigma_3 & \tau_{12} & \tau_{23} & \tau_{13} \end{bmatrix} \tag{30}$$

$$\varepsilon' = \begin{bmatrix} \varepsilon_1 & \varepsilon_2 & \varepsilon_3 & \gamma_{12} & \gamma_{23} & \gamma_{13} \end{bmatrix} \tag{31}$$

$$D = \frac{1}{\Delta} \begin{bmatrix} E_1(1-\nu_{23}\nu_{32}) & E_1(\nu_{21}+\nu_{31}\nu_{23}) & E_1(\nu_{31}+\nu_{21}\nu_{32}) & 0 & 0 & 0 \\ E_2(\nu_{12}+\nu_{13}\nu_{32}) & E_2(1-\nu_{13}\nu_{31}) & E_2(\nu_{32}+\nu_{12}\nu_{31}) & 0 & 0 & 0 \\ E_3(\nu_{13}+\nu_{12}\nu_{23}) & E_3(\nu_{23}+\nu_{21}\nu_{13}) & E_3(1-\nu_{12}\nu_{21}) & 0 & 0 & 0 \\ 0 & 0 & 0 & \Delta G_{12} & 0 & 0 \\ 0 & 0 & 0 & 0 & \Delta G_{23} & 0 \\ 0 & 0 & 0 & 0 & 0 & \Delta G_{13} \end{bmatrix} \tag{32}$$

$$\Delta = (1-\nu_{12}\nu_{21}-\nu_{23}\nu_{32}-\nu_{31}\nu_{13}-2\nu_{12}\nu_{23}\nu_{31}) \tag{33}$$

The relation between engineering and tensor strain vectors, along lamina and laminate axes, can be given as

$$\varepsilon' = R\varepsilon'_{ts} \tag{34}$$

$$\varepsilon^\circ = R\varepsilon^\circ_{ts} \tag{35}$$

where

$$R = \begin{bmatrix} 1 & 0 & 0 & 0 & 0 & 0 \\ 0 & 1 & 0 & 0 & 0 & 0 \\ 0 & 0 & 1 & 0 & 0 & 0 \\ 0 & 0 & 0 & 2 & 0 & 0 \\ 0 & 0 & 0 & 0 & 2 & 0 \\ 0 & 0 & 0 & 0 & 0 & 2 \end{bmatrix} \quad (36)$$

If the angle between lamina and laminate axes can be defined as α, then the lamina to laminate axis transformation is given by

$$T = \begin{bmatrix} c^2 & s^2 & 0 & 2sc & 0 & 0 \\ s^2 & c^2 & 0 & -2sc & 0 & 0 \\ 0 & 0 & 1 & 0 & 0 & 0 \\ -sc & sc & 0 & (c^2 - s^2) & 0 & 0 \\ 0 & 0 & 0 & 0 & c & -s \\ 0 & 0 & 0 & 0 & s & c \end{bmatrix} \quad (37)$$

where

$$c = \cos \alpha$$

$$s = \sin \alpha \quad (38)$$

and the stress and strain along the lamina and laminate axes can be equated as

$$\sigma' = T\sigma^\circ \quad (39)$$

$$\varepsilon'_{ts} = T\varepsilon^\circ_{ts} \quad (40)$$

By making use of Eqs. (34)–(40), one can get the laminate stress-strain relationship as

$$\sigma^\circ = Q\varepsilon^\circ \quad (41)$$

where

$$Q = T^{-1}D(T^{-1})^t \quad (42)$$

$$(T^{-1})^t = RTR^{-1} \quad (43)$$

$$Q = \begin{bmatrix} Q_{11} & Q_{12} & Q_{13} & Q_{14} & 0 & 0 \\ Q_{21} & Q_{22} & Q_{23} & Q_{24} & 0 & 0 \\ Q_{31} & Q_{32} & Q_{33} & Q_{34} & 0 & 0 \\ Q_{41} & Q_{42} & Q_{43} & Q_{44} & 0 & 0 \\ 0 & 0 & 0 & 0 & Q_{55} & Q_{56} \\ 0 & 0 & 0 & 0 & Q_{65} & Q_{66} \end{bmatrix} \quad (44)$$

$$Q_{11} = D_{11}c^4 + 2(D_{12} + 2D_{44})s^2c^2 + D_{22}s^4 \quad (45)$$

$$Q_{12} = D_{12}(s^4 + c^4) + (D_{11} + D_{22} - 4D_{44})s^2c^2 \quad (46)$$

$$Q_{13} = D_{31}c^2 + D_{32}s^2 \quad (47)$$

$$Q_{14} = (D_{11} - D_{12} - 2D_{44})sc^3 + (D_{12} - D_{22} + 2D_{44})s^3c \quad (48)$$

$$Q_{22} = D_{11}s^4 + 2(D_{12} + 2D_{44})s^2c^2 + D_{22}c^4 \quad (49)$$

$$Q_{23} = D_{13}s^2 + D_{23}c^2 \quad (50)$$

$$Q_{24} = (D_{11} - D_{12} - 2D_{44})s^3c + (D_{12} - D_{22} + 2D_{44})sc^3 \quad (51)$$

$$Q_{33} = D_{33} \quad (52)$$

$$Q_{34} = (D_{13} - D_{23})sc \quad (53)$$

$$Q_{44} = (D_{11} - 2D_{12} + D_{22} - 2D_{44})s^2c^2 + D_{44}(c^4 + s^4) \quad (54)$$

$$Q_{55} = D_{55}c^2 + D_{66}s^2 \quad (55)$$

$$Q_{56} = (D_{66} - D_{55})sc \quad (56)$$

$$Q_{66} = D_{55}s^2 + D_{66}c^2 \quad (57)$$

Appendix II. Coefficients of *C*-Matrix

$$\Phi = (Q_{22}Q_{44} - Q_{24}^2) \quad (58)$$

$$C_{11} = Q_{11} + \frac{Q_{12}}{\Phi}(Q_{14}Q_{24} - Q_{12}Q_{44}) + \frac{Q_{14}}{\Phi}(Q_{12}Q_{24} - Q_{14}Q_{22}) \quad (59)$$

$$C_{12} = Q_{13} + \frac{Q_{12}}{\Phi}(Q_{24}Q_{34} - Q_{23}Q_{44}) + \frac{Q_{14}}{\Phi}(Q_{23}Q_{24} - Q_{22}Q_{34}) \quad (60)$$

$$C_{21} = Q_{13} + \frac{Q_{23}}{\Phi}(Q_{14}Q_{24} - Q_{12}Q_{44}) + \frac{Q_{34}}{\Phi}(Q_{12}Q_{24} - Q_{14}Q_{22}) \quad (61)$$

$$C_{22} = Q_{33} + \frac{Q_{23}}{\Phi}(Q_{24}Q_{34} - Q_{23}Q_{44}) + \frac{Q_{34}}{\Phi}(Q_{23}Q_{24} - Q_{22}Q_{34}) \quad (62)$$

$$C_{33} = Q_{66} - \frac{Q_{56}^2}{Q_{55}} \quad (63)$$

Appendix III. Coefficients of *D*-Matrix

Using a binomial series, the following terms can be expanded as

$$\frac{1}{(1 + z/R)} = 1 - \frac{z}{R} + \frac{z^2}{R^2} - \frac{z^3}{R^3} \quad (64)$$

$$\frac{1}{(1 + z/R)^2} = 1 - \frac{2z}{R} + \frac{3z^2}{R^2} - \frac{4z^3}{R^3} \quad (65)$$

which are used in the evaluation of various *D* matrices

$$D_{aa} = b \int Z_a C_{11} Z_a^t \, dz = b \sum_{l=1}^{NL} C_{11} \begin{bmatrix} H_1 - \dfrac{2}{R}H_2 + \dfrac{3}{R^2}H_3 - \dfrac{4}{R^3}H_4 & H_3 - \dfrac{2}{R}H_4 + \dfrac{3}{R^2}H_5 - \dfrac{4}{R^3}H_6 \\[2mm] H_3 - \dfrac{2}{R}H_4 + \dfrac{3}{R^2}H_5 - \dfrac{4}{R^3}H_6 & H_5 - \dfrac{2}{R}H_6 + \dfrac{3}{R^2}H_7 - \dfrac{4}{R^3}H_8 \end{bmatrix} \tag{66}$$

$$D_{ab} = b \int Z_a C_{11} Z_b^t \, dz = b \sum_{l=1}^{NL} C_{11} \begin{bmatrix} H_2 - \dfrac{2}{R}H_3 + \dfrac{3}{R^2}H_4 - \dfrac{4}{R^3}H_5 & H_4 - \dfrac{2}{R}H_5 + \dfrac{3}{R^2}H_6 - \dfrac{4}{R^3}H_7 \\[2mm] H_4 - \dfrac{2}{R}H_5 + \dfrac{3}{R^2}H_6 - \dfrac{4}{R^3}H_7 & H_6 - \dfrac{2}{R}H_7 + \dfrac{3}{R^2}H_8 - \dfrac{4}{R^3}H_9 \end{bmatrix} \tag{67}$$

$$D_{ba} = D_{ab} \tag{68}$$

$$D_{bb} = b \int Z_b C_{11} Z_b^t \, dz = b \sum_{l=1}^{NL} C_{11} \begin{bmatrix} H_3 - \dfrac{2}{R}H_4 + \dfrac{3}{R^2}H_5 - \dfrac{4}{R^3}H_6 & H_5 - \dfrac{2}{R}H_6 + \dfrac{3}{R^2}H_7 - \dfrac{4}{R^3}H_8 \\[2mm] H_5 - \dfrac{2}{R}H_6 + \dfrac{3}{R^2}H_7 - \dfrac{4}{R^3}H_8 & H_7 - \dfrac{2}{R}H_8 + \dfrac{3}{R^2}H_9 - \dfrac{4}{R^3}H_{10} \end{bmatrix} \tag{69}$$

$$D_{at} = b \int Z_a C_{12} Z_t^t \, dz = b \sum_{l=1}^{NL} C_{12} \begin{bmatrix} H_1 - \dfrac{2}{R}H_2 + \dfrac{3}{R^2}H_3 - \dfrac{4}{R^3}H_4 & H_2 - \dfrac{2}{R}H_3 + \dfrac{3}{R^2}H_4 - \dfrac{4}{R^3}H_5 \\[2mm] H_3 - \dfrac{2}{R}H_4 + \dfrac{3}{R^2}H_5 - \dfrac{4}{R^3}H_6 & H_4 - \dfrac{2}{R}H_5 + \dfrac{3}{R^2}H_6 - \dfrac{4}{R^3}H_7 \end{bmatrix} \tag{70}$$

$$D_{bt} = b \int Z_b C_{12} Z_t^t \, dz = b \sum_{l=1}^{NL} C_{12} \begin{bmatrix} H_2 - \dfrac{2}{R}H_3 + \dfrac{3}{R^2}H_4 - \dfrac{4}{R^3}H_5 & H_3 - \dfrac{2}{R}H_4 + \dfrac{3}{R^2}H_5 - \dfrac{4}{R^3}H_6 \\[2mm] H_4 - \dfrac{2}{R}H_5 + \dfrac{3}{R^2}H_6 - \dfrac{4}{R^3}H_7 & H_5 - \dfrac{2}{R}H_6 + \dfrac{3}{R^2}H_7 - \dfrac{4}{R^3}H_8 \end{bmatrix} \tag{71}$$

$$D_{ta} = b \int Z_t C_{21} Z_a^t \, dz = b \sum_{l=1}^{NL} C_{21} \begin{bmatrix} H_1 - \dfrac{2}{R}H_2 + \dfrac{3}{R^2}H_3 - \dfrac{4}{R^3}H_4 & H_3 - \dfrac{2}{R}H_4 + \dfrac{3}{R^2}H_5 - \dfrac{4}{R^3}H_6 \\[2mm] H_2 - \dfrac{2}{R}H_3 + \dfrac{3}{R^2}H_4 - \dfrac{4}{R^3}H_5 & H_4 - \dfrac{2}{R}H_5 + \dfrac{3}{R^2}H_6 - \dfrac{4}{R^3}H_7 \end{bmatrix} \tag{72}$$

$$D_{tb} = b \int Z_t C_{21} Z_b^t \, dz = b \sum_{l=1}^{NL} C_{21} \begin{bmatrix} H_2 - \dfrac{2}{R}H_3 + \dfrac{3}{R^2}H_4 - \dfrac{4}{R^3}H_5 & H_4 - \dfrac{2}{R}H_5 + \dfrac{3}{R^2}H_6 - \dfrac{4}{R^3}H_7 \\[2mm] H_3 - \dfrac{2}{R}H_4 + \dfrac{3}{R^2}H_5 - \dfrac{4}{R^3}H_6 & H_5 - \dfrac{2}{R}H_6 + \dfrac{3}{R^2}H_7 - \dfrac{4}{R^3}H_8 \end{bmatrix} \tag{73}$$

$$D_{tt} = b \int Z_t C_{22} Z_t^t \, dz = b \sum_{l=1}^{NL} C_{22} \begin{bmatrix} H_1 & H_2 \\ H_2 & H_3 \end{bmatrix} \tag{74}$$

$$D_{ss} = b \int Z_s C_{33} Z_s^t \, dz = b \sum_{l=1}^{NL} C_{33} \begin{bmatrix} H_1 & H_3 & H_2 & H_4 \\ & H_5 & H_4 & H_6 \\ & & H_3 & H_5 \\ \textbf{Sym} & & & H_7 \end{bmatrix} \tag{75}$$

In Eqs. (66)–(75), for a given layer l

$$H_p = \frac{1}{p}(h_l^p - h_{l-1}^p) \tag{76}$$

where NL=total number of layers of a cross section; p=constant varying from 1 to 10; h_l=distance from the neutral axis to the top of a layer, l, and h_{l-1}=distance from the neutral axis to the top of layer $l-1$ or bottom of layer l.

Appendix IV. Shape Functions

The shape functions of isoparametric elements used in this study are presented as follows.

Linear Element

$$N_1 = (1.0 - \xi)/2 \tag{77}$$

$$N_2 = (1.0 + \xi)/2 \tag{78}$$

Quadratic Element

$$N_1 = (-\xi + \xi^2)/2 \tag{79}$$

$$N_2 = 1.0 - \xi^2 \tag{80}$$

$$N_3 = (\xi + \xi^2)/2 \tag{81}$$

Cubic Element

$$N_1 = (-1.0 + \xi + 9.0\xi^2 - 9.0\xi^3)/16 \tag{82}$$

$$N_2 = 9.0(1.0 - 3.0\xi - \xi^2 + 3.0\xi^3)/16 \tag{83}$$

$$N_3 = 9.0(1.0 + 3.0\xi - \xi^2 - 3.0\xi^3)/16 \tag{84}$$

$$N_4 = (-1.0 - \xi + 9.0\xi^2 + 9.0\xi^3)/16 \tag{85}$$

Notation

The following symbols are used in this paper:

BC = boundary condition;
FOST = first-order shear deformation theory of Timoshenko (1921);
HOAM = higher-order arch model;
k = shear correction factor = $5/6$;
M_0 = moment applied on the structure;
NDP = nondimensionalizing parameter; and
P_C = concentrated load;
P_S = magnitude of sinusoidal load $[P_S \sin(\Pi x/S)]$;
P_U = uniformly applied load;
R = radius of curvature;
S = arc length of the arch;
S/t = aspect ratio;
t = thickness of cross section; and
$\beta(=S/R)$ = subtended angle of an arch.

References

Allen, H. G. (1969). *Analysis and design of structural sandwich panels*, Pergamon Press, London.

Babu, C. R., and Prathap, G. (1986). "A linear thick curved beam element." *Int. J. Numer. Methods Eng.*, 23(7), 1313–1328.

Balasubramanian, T. S., and Prathap, G. (1989). "A field consistent higher-order curved beam element for static and dynamic analysis of stepped arches." *Comput. Struct.*, 33(1), 281–288.

Bathe, K. J. (1982). *Finite element procedures in engineering analysis*, Prentice-Hall, N.J.

Cevik, M. (2007). "An elastic-plastic thermal stress analysis of cross-ply and angle-ply aluminum metal-matrix composite arches." *J. Reinf. Plast. Compos.*, 26(2), 169–181.

Chen, J. K., and Sun, C. T. (1985). "Nonlinear transient responses of initially stressed composite plates." *Comput. Struct.*, 21(3), 513–520.

Choi, J. K., and Lim, J. K. (1995). "General curved beam elements based on the assumed strain fields." *Comput. Struct.*, 55(3), 379–386.

Cowper, G. R. (1966). "The shear coefficient in Timoshenko beam theory." *J. Appl. Mech.*, 33(2), 335–340.

Dawe, D. J. (1974a). "Curved finite elements for the analysis of shallow and deep arches." *Comput. Struct.*, 4(3), 559–580.

Dawe, D. J. (1974b). "Numerical studies using circular arch finite elements." *Comput. Struct.*, 4(4), 729–740.

Ganapathi, M., Patel, B. P., Saravanan, J., and Touratier, M. (1999). "Shear flexible curved spline beam element for static analysis." *Finite Elem. Anal. Design*, 32(3), 181–202.

Gere, J. M., and Weaver, W. (1965) *Analysis of Framed Structures*, D. Van Nostrand Company, New York, 450.

Jones, R. M. (1975). *Mechanics of composite materials*, McGraw-Hill Kogakusha, Tokyo.

Kikuchi, F., and Tanizawa, K. (1984). "Accuracy and locking free property of beam element for arch problems." *Comput. Struct.*, 19(1–2), 103–110.

Kim, D., and Chaudhuri, R. A. (2009). "Post buckling behavior of symmetrically laminated thin shallow circular arches." *Compos. Struct.*, 87(1), 101–108.

Krishnan, A., and Suresh, Y. J. (1998). "A simple cubic linear element for static and free vibration analyses of curved beams." *Comput. Struct.*, 68(5), 473–489.

Kulikov, G. M., and Plotnikova, S. V. (2004). "Non-conventional nonlinear two-node hybrid stress-strain curved beam elements." *Finite Elem. Anal. Design*, 40(11), 1333–1359.

Lee, H. P. (1969). "Generalized stiffness matrix of a curved-beam element." *AIAA J.*, 7(10), 2043–2045.

Lee, P. G., and Sin, H. C. (1994). "Locking-free curved beam element based on curvature." *Int. J. Numer. Methods Eng.*, 37(6), 989–1007.

Litewka, P., and Rakowski, J. (1998). "The exact thick arch finite element." *Comput. Struct.*, 68(4), 369–379.

Lo, K. H., Christensen, R. M., and Wu, E. M. (1977). "A higher-order theory of plate deformation. Part 1: Homogenous plates." *J. Appl. Mech.*, 44(4), 663–668.

Malekzadeh, P. (2009) "A two-dimensional layerwise-differential quadrature static analysis of thick laminated composite circular arches." *Appl. Math. Model.*, 33(4), 1850–1861.

Matsunaga, H. (2003). "Interlaminar stress analysis of laminated composite and sandwich circular arches subjected to thermal/ mechanical loading." *Compos. Struct.*, 60(3), 345–358.

Prathap, G. (1985). "The curved beam/deep arch/finite ring element revisited." *Int. J. Numer. Methods Eng.*, 21(3), 389–407.

Prathap, G., and Babu, C. R. (1986). "An isoparametric quadratic thick curved beam element." *Int. J. Numer. Methods Eng.*, 23(9), 1583–1600.

Prathap, G., and Babu, C. R. (1987). "Field-consistency and violent stress oscillations in the finite element method." *Int. J. Numer. Methods Eng.*, 24(10), 2017–2033.

Prathap, G., and Shashirekha, B. R. (1993). "Variationally correct assumed strain field for the simple curved beam element." *Comput. Struct.*, 47(6), 1071–1073.

Qatu, M. S. (2004). *Vibration of laminated shells and plates*, Elsevier, Oxford.

Raveendranath, P., Singh, G., and Pradhan, B. (2000). "Application of coupled polynomial displacement fields to laminated beam elements." *Comput. Struct.*, 78(5), 661–670.

Reddy, J. N. (1982). "On the solutions to forced motions of rectangular composite plates." *J. Appl. Mech.*, 49(3), 403–408.

Saleeb, A. F., and Chang, T. Y. (1987). "On the hybrid-mixed formulation of C^0 curved beam elements." *Comput. Methods Appl. Mech. Eng.*, 60(1), 95–121.

Stolarski, H., and Belytschko, T. (1982). "Membrane locking and reduced integration for curved elements." *J. Appl. Mech.*, 49(1), 172–176.

Stolarski, H., and Belytschko, T. (1983). "Shear and membrane locking in curved C^0 elements." *Comput. Methods Appl. Mech. Eng.*, 41(3), 279–296.

Stolarski, H. K., and Chiang, M. Y. M. (1989). "The mode decomposition C^0 formulation of curved two-dimensional structural elements." *Int. J. Numer. Methods Eng.*, 28(1), 145–154.

Timoshenko, S. P. (1921). "On the correction for shear in differential equation for transverse vibrations of prismatic bars." *Philos. Mag.*, 41(6), 744–746.

Vinayak, R. U., Prathap, G., and Naganarayana, B. P. (1996). "Beam elements based on a higher-order theory. I: Formulation and analysis of performance." *Comput. Struct.*, 58(4), 775–789.